MINISTRY OF EDUCATION AND TRAINING
HCMC UNIVERSITY OF TECHNOLOGY AND EDUCATION

NGO BA VIET

COMBINING EEG SIGNALS, CAMERAS AND LANDMARKS TO LOCATE AND CONTROL THE ELECTRIC WHEELCHAIR TO THE DESTINATION BASED ON THE MAP

Major: Electronic Engineering
Major code: 9520203

SUMMARY OF PH.D. DISSERTATION

HO CHI MINH CITY – 2024

THIS DISSERTATION WAS COMPLETED AT

HCMC UNIVERSITY OF TECHNOLOGY AND EDUCATION

Supervisor: Associate Prof. NGUYEN THANH HAI

Reviewer 1:

Reviewer 2:

Reviewer 3:

The dissertation was presented at the primary committee at HCMC University of Technology and Education, on ……/……/ 2024

CONTRIBUTIONS OF THE DISSERTATION

The dissertation focuses on researching the construction of an autonomous control system for electric wheelchairs in indoor environments, based on the integration of EEG brain signals, camera systems, landmarks, and maps to reduce the level of control required by people with disabilities and enhance safety. Therefore, the new scientific contributions of the dissertation include:

1. Proposing a method for classifying EEG signals of eye-blink activities based on amplitude thresholding and a classification method using a 1D convolutional neural network (CNN-1D). Specifically, EEG signals of eye-blink activities are collected and preprocessed for the classification process. The amplitude thresholding classification method allows direct processing of EEG signals with short processing time and high accuracy. With the CNN-1D model, data needs to be collected beforehand for the training process. However, the CNN-1D network allows the classification of various types of eye blinks with higher accuracy.

2. Proposing a method for recognizing natural landmarks and determining their positions in indoor environments. During movement, with this method, landmarks do not need to be pre-learned; the wheelchair will autonomously recognize and select landmarks based on the feature density of objects in the environmental image. Subsequently, the wheelchair will calculate the position of the landmarks and then store them in the database. The process of collecting landmarks and their position information is performed quickly with high accuracy, forming the basis for wheelchair localization on the map.

3. Leveraging landmark information, the dissertation suggests a method for wheelchair localization on a virtual 2D grid map, facilitating accurate and swift wheelchair navigation to desired destinations. Specifically, by constructing a virtual 2D grid map from the real environment with empty and obstacle cells, the wheelchair needs to be localized for the proposed control system to find the optimal path to the destination. This position is calculated from the position of the landmark in the environmental space and in the 3D space of the camera. Using a single landmark for wheelchair localization is recommended for higher accuracy compared to using three landmarks.

4. Proposing a real-virtual control model for autonomous electric wheelchairs. The DQNs-PreLU model is recommended for training to find the optimal path for the wheelchair based on the virtual 2D grid map. The DQNs-PreLU model with selected parameters helps reduce training time while maintaining high accuracy. Furthermore, a control algorithm for wheelchairs in real environments derived from simulated paths on the grid map is also proposed.

CHAPTER 1: INTRODUCTION

1.1. Rationale of the research

In today's society, individuals with disabilities consistently encounter physical and mental challenges, with global statistics from the World Health Organization (WHO) in 2022 revealing that 16% of the world's population, equivalent to 1.3 billion people, are living with disabilities, a number on the rise [1]. In Vietnam, as of 2019, approximately 6.2 million people, constituting 7.06% of the population aged 2 and above, are reported to have disabilities, with 58% being female, 28.3% children, and nearly 29% having severe or profound disabilities [2]. Worldwide, around 7% of individuals with mobility disabilities rely on wheelchairs [3]. The electric wheelchair market generated 2.89 billion USD in revenue in 2021 and is anticipated to reach 5.27 billion USD, reflecting a growth of about 10.76% from 2022 to 2027 [4].

❖ **Scientific publications**

In Dr. Nguyen Thanh Hai's 2013 research project, 'Development of an Intelligent Electric Wheelchair using EEG Brainwave Technology and Camera Sensors for Severely Disabled Individuals,' an autonomous wheelchair model was created, featuring an EEG brainwave-controlled interface and an automatic obstacle avoidance system [5]. Dr. Lam Quang Chuyen's 2020 doctoral dissertation, 'Neural Network in the Control System of Wheelchairs for Severe Disabilities Using Electroencephalography (EEG) and Camera,' explored three EEG signal preprocessing methods: Fourier transform, Wavelet transform, and Hilbert Huang transform (HHT). These methods transformed signals into Delta, Theta, Alpha, Beta, and Gamma waveforms, followed by data clustering and input into a neural network for classifying five motion signals [6]. The best result achieved was 92.4% accuracy with the group of 20 individuals selected for the experiment.

In a 2016 study, Ana Lopes introduced a model suggesting shared control between the Brain-Computer Interface (BCI) P300 communication system and a planning algorithm to oversee real-time control of electric wheelchairs in real-world indoor environments [7]. Similarly, in another 2016 study by Zhijun Li, a human-machine control approach was proposed, integrating both Brain-Computer Interface (BCI) and automatic control modes to regulate wheelchair direction [8]. Jingsheng Tang, in his 2018 research, presented an enhanced mobile structure for wheelchairs, featuring a lightweight robotic arm, target recognition module, and automatic control module [9].

1.2. Research objectives

The dissertation aims to develop an autonomous control system for electric wheelchairs indoors, integrating EEG signals, cameras, landmarks, and maps to minimize user input and improve safety for individuals with disabilities. To achieve this main goal, specific objectives need to be accomplished:

1. Design an interface for communication between humans and computers using EEG signals from eye-blink activities to select desired destinations.

2. Propose a method for locating the electric wheelchair on a map based on the positions of landmarks in the environment. To achieve this, landmarks with their location information in the environment need to be collected. Therefore, a method for recognizing landmarks in the natural environment and determining their positions needs to be investigated.

3. Develop an autonomous control model for the wheelchair to reach the desired destination, minimizing the user's control involvement.

1.3. Problem and scope of research

❖ **Problem:**

- Researching methods for classifying eye-blink activities from EEG signals.
- Investigating algorithms for landmark recognition in natural environments.
- Exploring algorithms for positioning based on landmarks in natural environments.
- Studying automatic control algorithms for wheelchairs based on the integration of EEG signals, landmarks, and maps.

❖ **Research Scope:** The dissertation concentrates on the research of the control system for electric wheelchairs in indoor environments, targeting users with limited mobility in their hands, legs, or heads, while their eyes remain functional.

1.4. Scientific contributions and practical significance

❖ **Scientific contributions**

- Proposing a method for classifying EEG signals of eye-blink activities based on amplitude thresholding and a classification method using a 1D convolutional neural network (CNN-1D).
- Proposing a method for recognizing natural landmarks and determining their positions in indoor environments.
- Leveraging landmark information, the dissertation suggests a method for wheelchair localization on a virtual 2D grid map, facilitating accurate and swift wheelchair navigation to desired destinations.
- Propose a hybrid control model for autonomous electric wheelchairs, employing the DQNs-PreLU model to train optimal paths on a virtual 2D grid map. Implement a control algorithm for real environments derived from simulated paths on the grid map.

❖ **Practical significance**

The dissertation is practically significant in developing an autonomous electric wheelchair model for individuals with disabilities. Furthermore, the research findings are applicable for instructing students in the field of Biomedical

Engineering at Ho Chi Minh City University of Technology and Education.

CHAPTER 2: THEORETICAL FOUNDATIONS

2.1. Overview of EEG Signals

EEG is the electrical signal of brain activity, measured using instruments that record electric currents with electrodes attached to the head. The recorded electrical fluctuations correspond to the brain's activities, and these activities are related to signals from the cerebral cortex [10].

2.2. Classification of Activities Based on EEG Signals

2.2.1. Detection of Eye Activities Based on Amplitude Thresholding of EEG Signals [11, 12]

2.2.2. Classification of Eye Activities Using Neural Networks [6, 13]

2.2.3. EEG Signal Classification Using Convolutional Neural Network [14, 15]

2.3. Brain-Computer Interface (BCI)

Brain-Computer Interface (BCI) is becoming increasingly popular as a technology to assist and enhance human communication abilities [16] [17].

2.4. Electric Wheelchair Model for People with Disabilities

2.4.1. Smart Electric Wheelchair [18, 19]

2.4.2. Electric Wheelchair with Robotic Control System [20]

2.4.3. Integrated Electric Wheelchair with Smart Environment [21]

2.4.4. Electric Wheelchair with Obstacle Avoidance Feature [22]

2.4.5. Shared Control System for Electric Wheelchairs [23, 24]

2.5. Method for Constructing a 2D Grid Map for Indoor Robot Navigation

A 2D grid map is one of the crucial methods for representing the environment in the field of mobile robotics. The grid map divides the space into multiple grids with attributes such as uncertainty, free space, and obstacles [25].

2.6. Localization Methods for Mobile Robots

2.6.1. Position Estimation Methods [26, 27]

2.6.2. Landmark-Based Robot Localization Methods [28]

2.6.3. Localization Methods for Robots Using WIFI Systems [29]

2.7. Object Recognition Methods

2.7.1. Appearance-Based Recognition Methods [30]

2.7.2. Feature-Based Recognition Methods [31, 32]

2.7.3. Object Recognition Using Machine Learning Methods [33, 34]

2.8. Modeling and Control of Electric Wheelchairs

2.8.1. Dynamic Modeling [35]

2.8.2. Motion Control of Electric Wheelchairs

2.9. Path Planning Methods for Mobile Robots

2.9.1. Algorithm A* (A-star) [36]

2.9.2. Reinforcement Learning Methods [37, 38]

CHAPTER 3: CLASSIFYING EEG SIGNALS FROM EYE ACTIVITY FOR HUMAN-COMPUTER COMMUNICATION APPLICATIONS

3.1. EEG signals from eye blinking activity

There are three types of eye blinking: reflexive blinking, involuntary blinking, and voluntary blinking. The EEG signals of voluntary and involuntary eye blinking are illustrated in Figure 3.3.

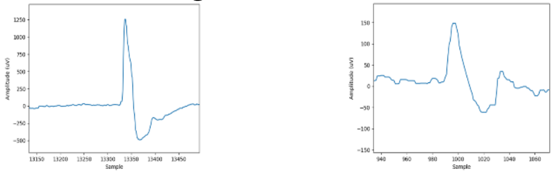

(a) Voluntary eye blinking signals (b) Involuntary eye blinking signals

Figure 3.3. *Two types of EEG signals from eye blinking activity.*

3.2. Data collection

The eye blinking signals are collected from 4 channels: AF3, F7, F8, and AF4. Each signal has a length of 701 samples. The data collection process is illustrated in Figure 3.6.

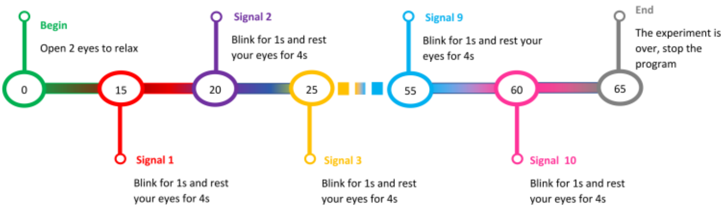

Figure 3.6. *Experimental procedure.*

3.3. Signal Processing

3.3.1. Filtering noise using a Hamming filter

The original signal will be passed through a Hamming filter. Figure 3.12 represents the filtered results of the original EEG signal using a Hamming filter.

3.3.2. Smoothing the signal using a Savitzky–Golay filter

The EEG signal before and after smoothing using a second-order Savitzky–Golay filter is presented in Figure 3.13. Figure 3.14 shows the smoothed EEG signal of eye blinking activity using a second-order Savitzky–Golay filter with window lengths of 7, 11, and 15.

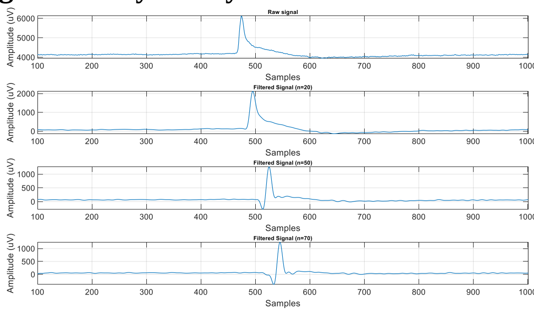

Figure 3.12. *The EEG signal from channel F7 during left eye blinking activity before and after filtering using a Hamming filter.*

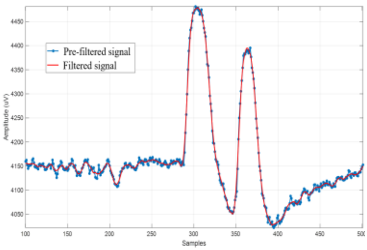

Figure 3.13. *The EEG signal at channel F7 before and after smoothing with a Savitzky-Golay filter.*

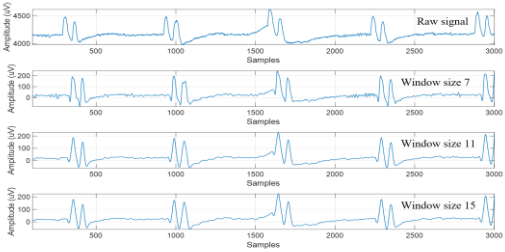

Figure 3.14. *The EEG signal from both eye blinking activity at channel F7, filtered with a Hamming filter and smoothed using a Savitzky-Golay filter.*

3.4. Classification of EEG signals from eye activity

3.4.1. Eye blinking activity classification through amplitude thresholding

❖ Amplitude thresholding method

The eye blinking signals will be segmented into frames as shown in Figure 3.15. The voluntary eye blinking signals exhibit characteristics as illustrated in Figure 3.16, including positive and negative peaks [39].

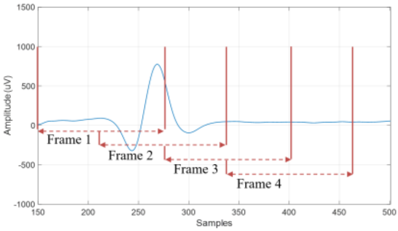

Figure 3.15*. Description of the method for segmenting EEG signals into data frames.*

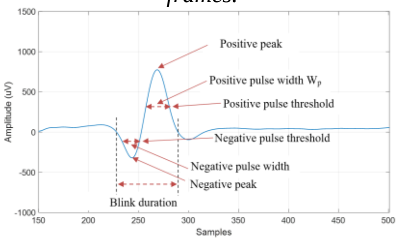

Figure 3.16*. Description of voluntary eye blinking signals.*

Algorithm 3.1: Blink detection

Input:
- *Y[n]*: processed EEG signal for a frame
- T_{AP}: amplitude threshold for positive pulse
- T_{AN}: amplitude threshold for negative pulse
- T_{WP}: width threshold for positive pulse
- T_{WN}: width threshold for negative pulse

for n = 1: N **do**
  if $Y[n] \geq T_{AP}$ **then**
    $Timer\_count\_positive++$
  else if $Y[n] \leq T_{AN}$ **then**
    $Timer\_count\_negative++$
end for
  $W_P = Timer\_count\_positive$
  $W_N = Timer\_count\_negative$
if $W_P \geq T_{WP}$ **then**
    $peak^+ = 1$
end if
if $W_N \geq T_{WN}$ **and** $peak^+ = 1$ **then**
  Blink
Else
  Not blinking
end if
Output: Blinking activity.

If Y[n] is referred to as the EEG signal of a frame, then the thresholds T_{AP} and T_{AN} are computed using the following formulas:

$$T_{AP} = \frac{max(Y[n])+min(Y[n])}{2} \quad , với\ Y[n] \geq 0 \tag{3.11}$$

$$T_{AN} = \frac{max(Y[n])+min(Y[n])}{2} \quad , với\ Y[n] < 0 \tag{3.12}$$

Algorithm 3.1 describes the method for detecting eye blinking activity.

❖ Classification results of blink activity based on amplitude threshold

Table 3.1. *Cases of eye activity classification.*

No.	Blinking at channel F7	Blinking at channel F8	Type of eye activity
1	Yes	No	Left eye blink
2	No	Yes	Right eye blink
3	No	No	Not blinking

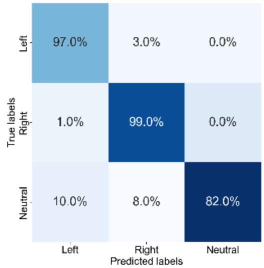

Figure 3.17. *Result of eye activity classification.*

Post-preprocessing, signals from F7 and F8 electrodes will identify left and right eye blinks according to Table 3.2. Classification results encompass left eye blinks, right eye blinks, and no blinks, illustrated in Figure 3.17.

3.4.2. Classifying eye activity signals using a 1D CNN model

❖ Creating a database

Figures 3.19, 3.21, 3.23, 3.25, and 3.27 depict synthesized signals from 4 channels (AF3, F7, F8, and AF4) containing 2804 samples, representing activities like left eye blinking, right eye blinking, both eyes blinking, both eyes blinking consecutively twice, and no blinking. These signals will be stored in the dataset for classification training.

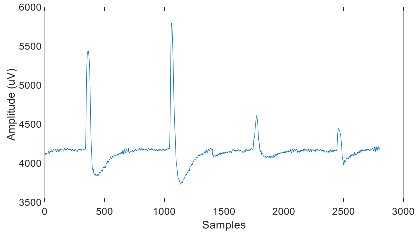

Figure 3.19. *The signal synthesized from 4 channels, with a length of 2804 samples, represents the left eye blinking activity.*

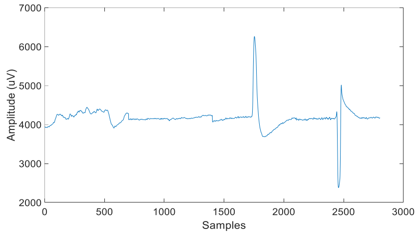

Figure 3.21. *The signal synthesized from 4 channels, with a length of 2804 samples, represents the right eye blinking activity.*

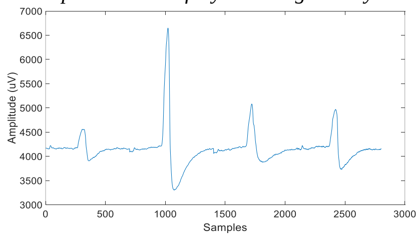

Figure 3.23. *The signal synthesized from 4 channels, with a length of 2804 samples, represents the activity of both eyes blinking.*

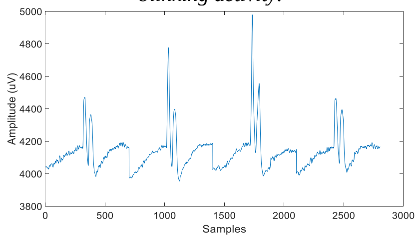

Figure 3.25. *The signal synthesized from 4 channels, with a length of 2804 samples, represents the activity of both eyes blinking consecutively twice.*

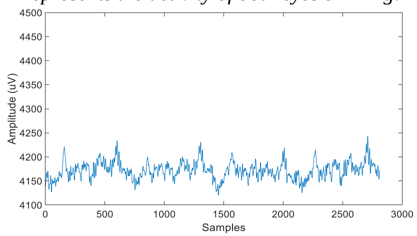

Figure 3.27. *The signal synthesized from 4 channels, with a length of 2804 samples, represents the activity of no blinking.*

❖ CNN-1D model

This study proposes a CNN-1D model with a structure as shown in Figure 3.28. The parameters and kernel sizes were determined through trial and error.

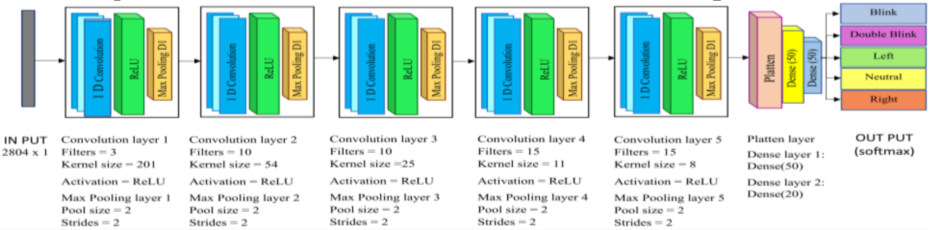

Figure 3.28. *The CNN-1D model for classifying EEG signals related to eye activity.*

❖ Evaluation methods for the classification model

In this dissertation, a confusion matrix is used to assess the accuracy of the classification model, as shown in Figure 3.29.

❖ Classification results of EEG signals using the CNN-1D model

Training data for the model, categorizing eye activities, is partitioned based on the ratios illustrated in Figure 3.30. Table 3.3 furnishes detailed data distribution for training and testing across various training scenarios.

		Predicted Class	
		Positive	*Negative*
Actual class	*Positive*	True Positive (TP)	False Negative (FN)
	Negative	False Positive (FP)	True Negative (TN)

Figure 3.29. *Confusion matrix.*

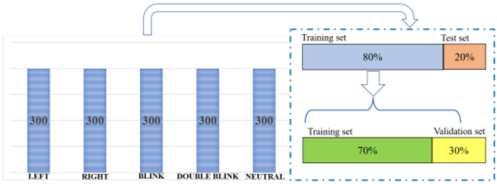

Figure 3.30. *Organization of data for training*

Table 3.3. *Description of the training data for eye activity classification.*

Various types of eye activities	Number of training data					Number of test data				
	L	R	B	DB	N	L	R	B	DB	N
L-R-N	240	240			240	60	60			60
L-R-B-N	240	240	240		240	60	60	60		60
L-R-B-DB-N	240	240	240	240	240	60	60	60	60	60

Figure 3.31 illustrates the training performance of the classification model for three blinking cases. Table 3.4 provides detailed performance descriptions of the CNN-1D model for various scenarios.

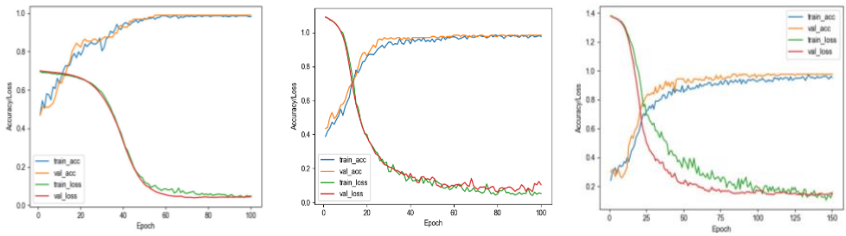

(a) Three types of eye blinks (b) Four types of eye blinks (c) Five types of eye blinks

Figure 3.31. *The training performance of the CNN-1D model for eye activity classification.*

__Table 3.4.__ Performance of the model during training for the classification of eye activities.

Type of eye activity	Epochs	Learning rate	ACC (%)	PRE (%)	SEN (%)
L – R – N	150	0,0001	99,38	99,39	99,38
			98,15	98,25	98,15
			98,77	98,81	98,77
			98,77	98,81	98,77
			98,77	98,77	98,77
L – R – B – N	150	0,0001	97,16	97,15	97,17
			98,58	98,59	98,61
			98,10	98,11	98,15
			97,16	97,23	97,22
			97,63	97,62	97,64
L – R – B – DB – N	150	0,0001	96,60	96,61	96,63
			98,49	98,50	98,44
			97,74	97,72	97,74
			97,36	97,41	97,33
			97,36	97,50	97,33

Table 3.5 and Figure 3.3 detail the performance of the model with EEG signals individually collected from 4 channels without signal fusion [40].

__Table 3.5.__ Five-fold cross-validation for the eye blink activity classifier.

	5-fold cross validation				
	1	*2*	*3*	*4*	*5*
ACC (%)	92,9	92,9	92,9	90,5	92,9
SEN (%)	94,1	88,9	94,4	89,5	94,1
PRE (%)	88,9	94,1	89,5	89,5	88,9

Results of eye blink classification as shown in Figure 3.32 and 3.33.

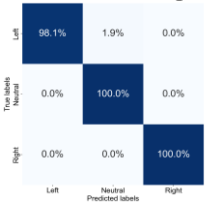

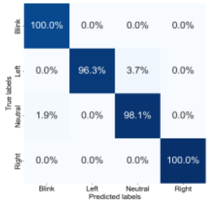

(a) Three types of blinks (b) Four types of blinks

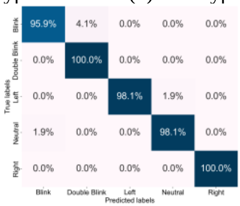

(c) Five types of blinks

__Figure 3.32.__ Classification results of eye activities by the model on the test set.

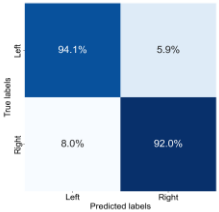

__Figure 3.33.__ Classification results of eye activities with left and right eye blinks using the unfused channel signals.

Table 3.6 compiles the results of recent studies on eye activity classification using EEG.

__Table 3.6.__ Studies on eye activity classification.

Works	Type of eye activity	Classification technique	Accuracy
Dang-Khoa Tran [11]	Left eye blink Right eye blink Blinking with both eyes	Peak threshold	95,1% 96,1% 97,2%
Kleifges K [41]	Blinking	Peak threshold	93,46%
M. Benda [42]	Blinking	Alpha peak detection	89.69%
Thanh-Hai Nguyen [13]	Open eyes Blinking with both eyes Left-eye squint Right-eye squint	Neural network (NN)	90% 97% 92% 95%
Proposed method 1	Left eye blink Right eye blink No blinking	Amplitude threshold	97% 99% 82%
Proposed method 2	Left eye blink Right eye blink Blinking with both eyes once Blinking with both eyes twice No blinking	CNN-1D	98,1% 100% 95,9% 100% 98,1%

CHAPTER 4: RECOGNITION AND POSITIONING OF NATURAL LANDMARKS IN INDOOR ENVIRONMENTS

4.1. The role of landmarks in the localization and control of electric wheelchairs

With mobile platforms, selecting landmarks and extracting their features for recognition plays a crucial role.

4.2. The maximum feature density method for recognizing landmarks in natural environments

To recognize natural landmarks in an image, the maximum feature density method is divided into three stages, as illustrated in Figure 4.1 [43].

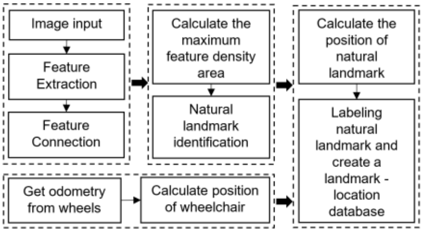

Figure 4.1. *The steps for recognizing natural landmarks.*

4.2.1. Feature extraction

To detect keypoints, the ORB detector is applied to accelerate feature extraction [44].

4.2.2. Connecting keypoints within objects

The keypoints of the object in the image are connected by dilating them. Specifically, the dilation of a binary image **A** with a structuring element **K** is performed, calculated as follows:

$$\boldsymbol{D} = \boldsymbol{A} \oplus \boldsymbol{K} = \left\{ z \,\middle|\, \left(\hat{\boldsymbol{K}}\right)_z \cap A \neq \Phi \right\} \quad (4.2) \qquad \boldsymbol{K} = \begin{bmatrix} 0 & 1 & 0 \\ 1 & 1 & 1 \\ 0 & 1 & 0 \end{bmatrix} \quad (4.3)$$

where $\left(\hat{\boldsymbol{K}}\right)_z$ is the projection of **K** from the origin and translated along **Z**. Therefore, the dilation of **A** with **K** is the set of all **Z** projections, such that $\left(\hat{\boldsymbol{K}}\right)_z$ and **A** overlap at least one element.

4.2.3. Recognizing natural landmarks

The dilated image **D** is processed to contain only 2 values, 0 and 1, and the sum of white pixels along row *r* and column *c* is determined according to formula (4.4). The sum of white pixels within the objects of the image $\mathbf{O_i}$ after drawing boundaries is calculated using formula (4.5).

$$\chi = \sum_{x=0}^{r} \sum_{y=0}^{c} \boldsymbol{D}(x, y) \quad (4.4) \qquad \chi_i = \sum_{x_i=0}^{h} \sum_{y_i=0}^{w} \boldsymbol{O_i}(x_i, y_i) \quad (4.5)$$

The feature point density coefficient on an object δ_i is determined according to equation (4.6). Subsequently, the object with the highest coefficient δ_i is selected as the natural landmark in the original image.

$$\delta_i = \frac{\chi_i}{\chi} \quad (4.6)$$

4.3. Determining the position of the landmark in the environment

4.3.1. The position of the wheelchair in the environment

The kinematic equation relates Cartesian coordinates O(x,y) of the wheelchair in the coordinate system to the velocities of its two wheels, as shown in Figure 4.2.

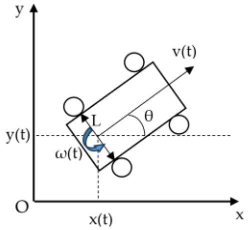

Figure 4.2. *A mobile wheelchair model with two differential wheels and two free caster wheels.*

The wheelchair in Figure 4.2 moves and orients itself by adjusting the velocities of the left wheel, $v_l(t)$, and the right wheel, $v_r(t)$. Using L as the distance between the wheels and θ as the angle between the frame axis and the horizontal axis, the coordinates $x(t)$, $y(t)$, and angle $\theta(t)$ at time t are determined as follows:

$$\begin{bmatrix}\dot{x}(t)\\ \dot{y}(t)\\ \dot{\theta}(t)\end{bmatrix} = \begin{bmatrix}\cos\theta(t) & 0\\ \sin\theta(t) & 0\\ 0 & 1\end{bmatrix}\begin{bmatrix}v(t)\\ \omega(t)\end{bmatrix} \quad (4.9)$$

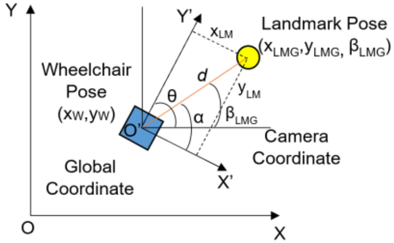

Figure 4.3. *Estimating the position of landmarks in 2D space .*

The coordinates of the wheelchair at time $t = k + 1$ are described as:

$$\begin{bmatrix}x(k+1)\\ z(k+1)\\ \theta(k+1)\end{bmatrix} = \begin{bmatrix}\cos\theta(k+1) & 0\\ \sin\theta(k+1) & 0\\ 0 & 1\end{bmatrix}\begin{bmatrix}\frac{d_r(k+1)+d_l(k+1)}{2}\\ \frac{d_r(k+1)-d_l(k+1)}{L}\end{bmatrix} + \begin{bmatrix}x(k)\\ z(k)\\ \theta(k)\end{bmatrix} \quad (4.10)$$

in which $d_r(k + 1)$ and $d_l(k + 1)$ represent the distances traveled by the right and left wheels from time k to $(k + 1)$, respectively.

4.3.2. Determining the position of the landmark

Figure 4.3 depicts the positions of the wheelchair and landmarks in space, where the coordinates of the wheelchair in the 2D environment are (x_W, y_W), and the coordinates of the landmark in the camera space are (x_{LM}, y_{LM}).

$$x_{LMG} = x_W + d.\cos\beta_{LMG} \quad (4.11) \qquad \beta_{LMG} = \alpha + \theta - 90 \quad (4.13)$$

$$y_{LMG} = y_W + d.\sin\beta_{LMG} \quad (4.12)$$

in which θ is the angle of the wheelchair's movement using equation (4.10). The angle of the landmark, α, is calculated as follows:

$$\alpha = \begin{cases} \arctan\left(\frac{y_{LM}}{x_{LM}}\right), & x_{LM} < 0\\ 180 - \arctan\left(\frac{y_{LM}}{x_{LM}}\right), & x_{LM} \geq 0\end{cases} \quad (4.14) \qquad d = \sqrt{{x_{LM}}^2 + {y_{LM}}^2} \quad (4.15)$$

Once the landmark position is established, the index and coordinates of the landmark in the image are marked and stored in the database.

4.4. The results of natural landmark recognition and data collection

In the experiment, the wheelchair is equipped with an RGB-D camera and two encoders, as shown in Figure 4.4.

Table 4.1 illustrates the performance of SIFT, SURF, and ORB detectors when extracting features from Figure 4.5. Figure 4.6 demonstrates the connectivity of keypoints of the objects in Figure 4.5, with keypoints dilation performed through various iterations. Figure 4.7 describes an image containing object boundaries and feature frames.

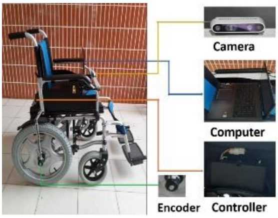

Figure 4.4. *Wheelchair with RGB-D camera, encoders, and computer.*

(a) RGB image (b) Image with key points

Figure 4.5. *Objects with corner feature.*

Table 4.1. *Feature extraction results using various methods.*

Detector	Time Per Frame (ms)	Time Per KeyPoint (ms)	Number of Key Points in Frame
SIFT [31]	31,08	0,07	426
SURF [32]	17,55	0,08	230
ORB [44]	3,74	0,002	1850

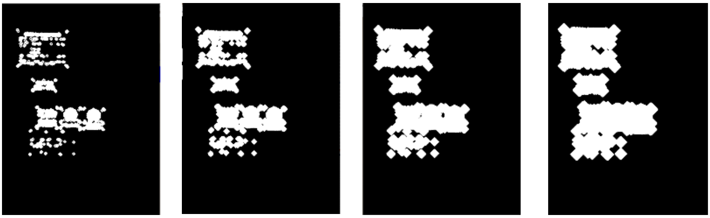

(a) One iteration (b) Five iterations (c) Ten iterations (d) Fifteen iterations

Figure 4.6. *Representation of dilation with different iterations using a 3x3 kernel.*

(a) One iteration (b) Five iterations (c) Ten iterations (d) Fifteen iterations

Figure 4.7. *Object contours and feature frames.*

In Figures 4.8 and 4.9, the image recognition system shows objects at distances of 2m and 1m from the camera to the wall. Figure 4.9c demonstrates that the second object is selected as the landmark corresponding to the highest density $\delta_2 = 0.85$ compared to the other object.

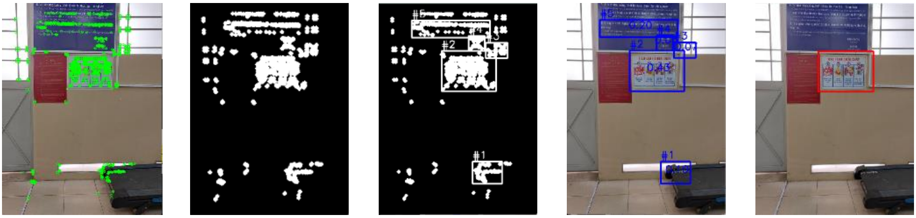

(a) Image with key points (b) Dilated image. (c) Feature frame (d) Objects image (e) Landmark image

Figure 4.8. *The process of landmark recognition in the laboratory at a distance of 2m from the camera to the objects.*

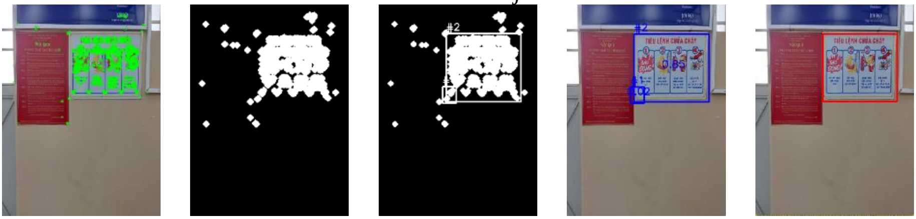

(a) Image with key points (b) Dilated image. (c) Feature frame (d) Objects image (e) Landmark image

Figure 4.9. *The process of landmark recognition in the laboratory at a distance of 1m from the camera to the objects.*

Figure 4.10 illustrates the IOU between two boxes: one encompassing the actual object and the other containing the landmark identified by the proposed algorithm. Table 4.2 presents the IOU at various distances.

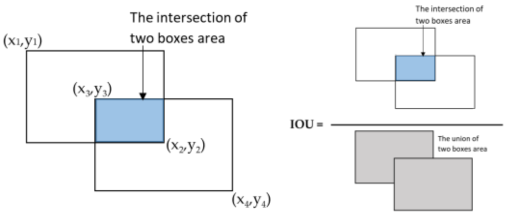

(a) Intersection of two boxes. (b) The IOU calculation.

Figure 4.10. *IOU for bounding boxes.*

Table 4.2. *IOU at different distances.*

No.	1m	2m	3m	4m	5m
1	0,86	0,83	0,72	0,56	0,68
2	0,90	0,92	0,57	0,61	0,50
3	0,91	0,83	0,53	0,55	0,48
4	0,86	0,85	0,56	0,54	0,47
5	0,89	0,91	0,55	0,63	0,60
6	0,80	0,90	0,55	0,58	0,28
7	0,80	0,80	0,57	0,49	0,56
8	0,88	0,83	0,55	0,47	0,48
9	0,86	0,86	0,55	0,55	0,60
10	0,80	0,85	0,63	0,62	0,56
Average	**0,86**	**0,86**	**0,58**	**0,56**	**0,52**

Table 4.3 describes the experiment of detecting landmarks in Figure 4.11 under various lighting conditions and at different distances.

Table 4.3. *IOU under different lighting conditions.*

Distance	**Standard lighting**		**Low light**		**Dark**	
	Landmark 1	**Landmark 2**	**Landmark 1**	**Landmark 2**	**Landmark 1**	**Landmark 2**
1 m	0,84	0,86	0,82	0,85	0,84	0,86
2 m	0,84	0,82	0,90	0,80	0,90	0,82
3 m	0,77	0,59	0,70	0,50	0,51	0,45

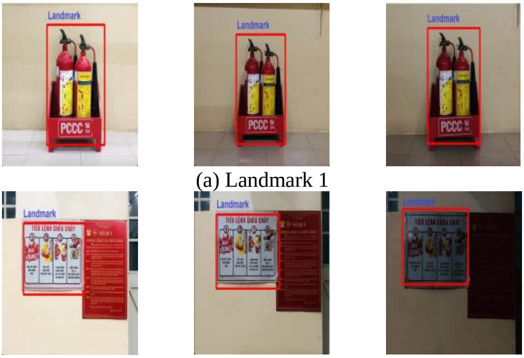

(a) Landmark 1

(b) Landmark 2

Figure 4.11. Recognition of natural landmarks in a laboratory environment under different lighting conditions.

The images of objects captured by the camera system at angles of 0°, 35°, and 45° are shown in Figures 4.12, 4.13, and 4.14, respectively.

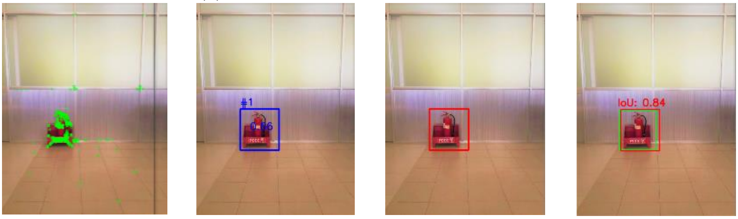

(a) Image with key points (b) Objects image (c) Landmark image (d) Bounding box with IOU ratio

Figure 4.12. Recognition of the natural landmark in the lab environment at the angle of 0°.

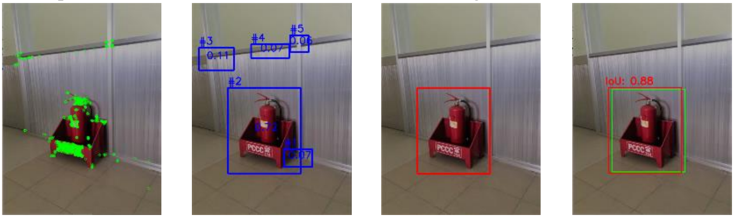

(a) Image with key points (b) Objects image (c) Landmark image (d) Bounding box with IOU ratio

Figure 4.13. Recognition of the natural landmark in the lab environment at the angle of 45°.

Table 4.4 displays the average processing time for each step, while Figure 4.15 showcases the outcomes of identifying landmarks in an indoor environment.

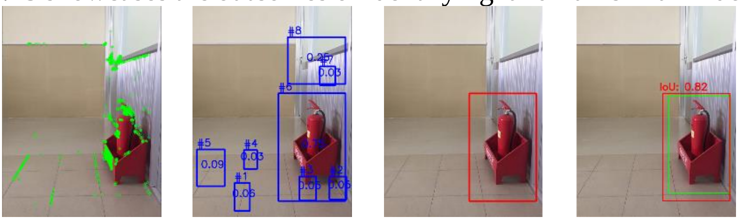

(a) Image with features. (b) Image of the objects. (c) The recognized landmark. (d) Bounding box with IOU ratio.

Figure 4.14. Recognition of the natural landmark in the lab environment at the angle of 30°.

***Table 4.4.** Processing time for landmark recognition of the proposed method.*

Stages of Implementation	Figure 4.15a	Figure 4.15c	Figure 4.15e	Figure 4.15g
Feature extraction [ms]	2,90	3,77	2,89	4,77
Object detection and landmark recognition [ms]	37,10	37,93	36,12	41,16
Total [ms]	40,00	41,70	39,01	45,93

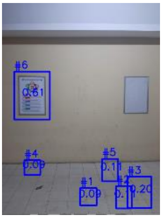

(a) Image frames on the wall in the corridor

(b) Recognized landmark

(c) Image frames on another wall in the corridor

(d) Recognized landmark

(e) Image frames on the wall of the lab room

(f) Recognized landmark

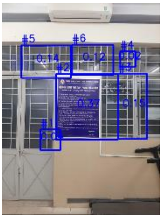

(g) Image frames on another wall of the lab room

(h) Recognized landmark

Figure 4.15. *Natural landmarks detected from various areas.*

4.5. Results of landmark position

In Figure 4.16, the relative error between the average measured distance and the actual distances of landmarks is depicted, each position being measured 100 times. The next experiment involves determining the positional error of the wheelchair in 2D space, as shown in Figure 4.17.

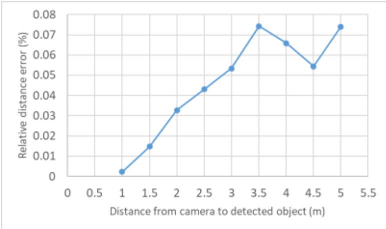

Figure 4.16. *The relative distance of the detected landmarks measurement error.*

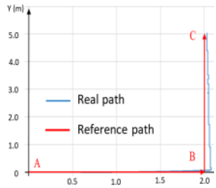

(a) Experiment 1

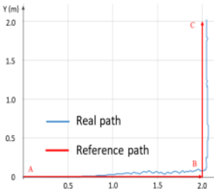

(b) Experiment 2

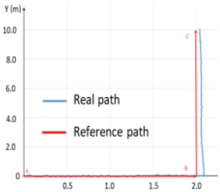

(c) Experiment 3

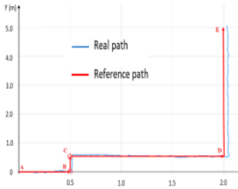

(d) Experiment 4

Figure 4.17. *Representation of the wheelchair's motion trajectory to pre-set positions.*

Positional errors of the wheelchair in three experiments (Figure 4.17a, 4.17b, and 4.17c) are outlined in Table 4.5. Figure 4.17d displays the actual trajectory (in green) and the reference trajectory (in red) of the wheelchair, while Table 4.6 details the outcomes of landmark position determination in various experiments.

Table 4.5. *Evaluation of wheelchair position error – Unit: cm.*

No.	Ground Truth	Actual Position	|Δx|	|Δy|
1	(200,0; 500,0)	(203,0; 502,0)	3,0	2,0
2	(200,0; 200,0)	(204,0; 201,0)	4,0	1,0
3	(200,0; 100,0)	(201,0; 99,0)	1,0	1,0

The method can be utilized to create an automated tool for labeling indoor landmark positions. Table 4.7 compiles studies on image object recognition and automatic acquisition of object location information.

Table 4.6. *Results of landmark localization based on wheelchair position – Unit: cm.*

Wheelchair position (x_w, y_w, θ_w)	**Distance to the landmark**	**Actual landmark position**	**Computed landmark position**	**|Δx|**	**|Δy|**
(30,0; 30,0; 90)	96,8	(60,6; 121,1)	(63,1; 120,9)	2,5	0,2
(30,0; 30,0; 45)	85,9	(90,7; 90,7)	(92,2; 89,2)	1,5	1,5
(40,0; 40,0; 60)	112,7	(120,0; 120,0)	(119,5; 119,9)	0,5	0,1
(40,0; 40.0; 30)	111,0	(120,0; 120,0)	(128,6; 106,9)	8,6	13,1
(80,0; 40,0; 120)	89,1	(40,0; 120,0)	(38,7; 119,0)	1,3	1,0
(60,5; 60,5; 90)	94,4	(85,0; 151,4)	(82,4; 152,3)	2,6	0,9
(324,8; 116,6; 45)	207,0	(495,2; 124,2)	(511,1; 206,9)	15,9	7,3

Table 4.7. *Automatic labeling system for objects overview.*

Works	**Objects**	**Object Detection Technique**	**Dataset for Pretraining**	**Processing Time**	**Description of the Collected Dataset**
X. Chai [45]	Doors, walls, ceilings, and floor	Object segmentation	Do not use	75 ms	Landmarks in an indoor environment
P. Du [46]	Tables, chairs, and low ceilings	YOLOv3	Millar Library	-	Objects with their longitude and latitude
Apud Baca [47]	Toys	CNNs	MS COCO	40 s	A six-degrees-of-freedom (6-DoF) posture of objects
O. Deane [48]	Mobile eye-tracking data	Mask R-CNN	MS COCO	1,5 s	Gaze coordinates
García-Aguilar [49]	Vehicles	EfficientDet D4	COCO	-	Objects with their coordinates in image
Proposed Method	Natural landmark	Maximum feature density	Do not use	41,66 ms	Landmarks and their position in indoor environment

CHAPTER 5: ELECTRIC WHEELCHAIR CONTROL MODEL INTEGRATING EEG SIGNALS AND CAMERA BASED ON MAP

5.1. Virtual-real control model for an electric wheelchair based on a virtual 2D grid map

5.1.1. The structure of the virtual-real control model for an electric wheelchair

In this dissertation, a virtual-real control model for an electric wheelchair is proposed to navigate the it to the desired destination [50], as illustrated in Figure 5.1.

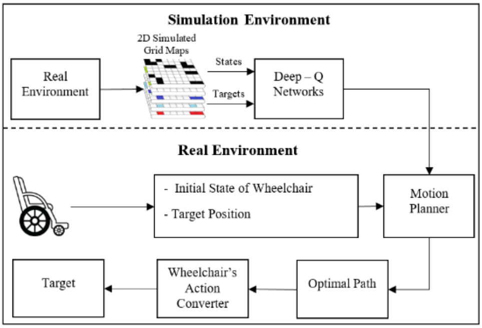

Figure 5.1. *Hệ thống điều khiển thực - ảo cho xe lăn điện dựa trên bản đồ lưới 2D ảo.*

5.1.2. Virtual 2D grid map.

Figure 5.3 depicts the virtual 2D grid map consisting of $m \times n$ grid cells in the indoor environment that the wheelchair can traverse to reach the destination.

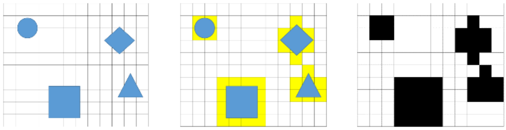

(a) Environment grid map with real obstacles and cells

(b) Occupied cells related to the real obstacles

(c) Virtual 2D grid map with black occupancy cells

Figure 5.3. *The 2D grid map of the real environment.*

5.1.3. Graphical user interface for selecting the destination

Figure 5.4 depicts the collection, processing, and classification of EEG signals for executing control commands related to the user interface [39, 40, 51]. Figures 5.5 and 5.6 display the graphical user interface.

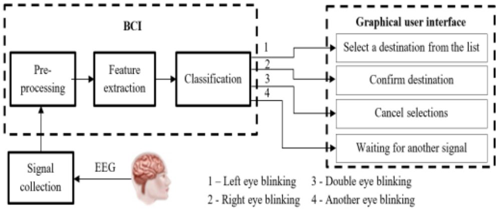

Figure 5.4. *Brain–computer interface process flow.*

Figure 5.5. *User interface for selecting the desired destination.*

Figure 5.6. *User interface selected the desired destination "Bed Room" using EEG.*

5.1.4. The DQNs model plans the optimal path for the wheelchair

Positions on the 2D grid map include three types: obstacle positions S_o, free space positions S_f, and the target destination S_g. At each time step t, the wheelchair is at position S_t and needs to choose an action from a predetermined set of actions. Furthermore, after each action, the wheelchair will move from the current position S_t to a new position S_{t+1} at time $(t + 1)$ and then the reward received after each action is $R(s_t,a_t) \in [-1,1]$. The policy π for position S_t will select an action to maximize the total reward Q obtained by the wheelchair.

$$\pi(s_t) = arg \max_{i=0,1,\dots,n} Q(s_t,a_i) \quad (5.2) \qquad Q(s_t,a_t) = R(s_t,a_t) + \gamma . \max_{i=0,1,\dots,n} Q(s_{t+1},a_i) \quad (5.3)$$

with $Q(s_t,a_i)$ being the reward when performing action a_i at position S_t; n is the number of actions; s_{t+1} is the next state; and γ is the discount factor.

To approximate $Q(s_t, a_t)$, the FWNN takes the position of the wheelchair on the grid map as input, and its output is a **Q**-value vector. Additionally, Q_i is the approximate value of $Q(s_t,a_{ti})$ for each action a_{ti}. When the neural network is trained sufficiently and accurately, it will be used in the optimal path planning model to select the policy π as the following equation:

$$\pi(s_t) = a_j \quad (5.4) \qquad j = arg \max_{i=0,1,\dots,n} Q_i \quad (5.5)$$

where the value of j is determined based on the maximum Q-value.

The purpose of the neural network is to accurately estimate the Q-values for various actions. Therefore, the objective function is:

$$Loss = \left(R(s_t, a_t) + \gamma \max_{a_{t+1}} Q(s_{t+1}, a_{t+1}) - Q(s_t, a_t) \right)^2 \qquad (5.6)$$

In this study, the PreLU activation function, RMSProp optimization method, and MSE loss function are applied.

5.2. Wheelchair localization using natural landmarks on a virtual 2D grid

As the wheelchair navigates the real environment with pre-selected landmarks (Figure 5.8), the camera, when identifying these landmarks, provides their positions in relation to the camera's location (Figure 5.9) [52].

Figure 5.8. *Samples of landmarks in the indoor environment.*

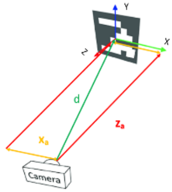

Figure 5.9. *Coordinate system of the RGB-D camera.*

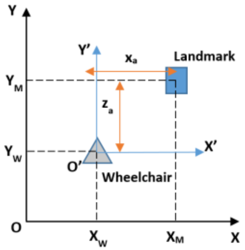

(a) Up direction of landmark

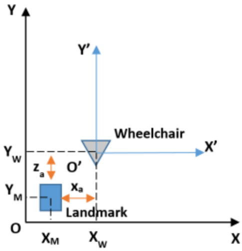

(b) Down direction of landmark

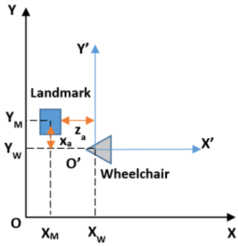

(c) Left direction of landmark

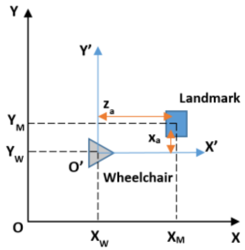

(d) Right direction of landmark

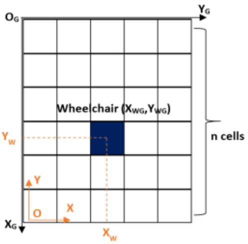

(e) The 2D grid map and in the OXY plane

Figure 5.10*. Positions of the wheelchair with four directions.*

Figure 5.10 illustrates the coordinate systems OXY in the 2D plane and the camera coordinate system O'X'Y'. In this study, the wheelchair's position in the 2D plane according to the OXY coordinate system is calculated as follows:

- The orientation of the landmark is "Up" in the 2D grid map:
- The orientation of the landmark is "Down" in the 2D grid map:

$$X_W = X_M - x_a \qquad Y_W = Y_M - z_a \tag{5.9}$$

$$X_W = X_M + x_a \qquad Y_W = Y_M + z_a \tag{5.10}$$

- The orientation of the landmark is "Right" in the 2D grid map:

$$X_W = X_M - z_a \qquad Y_W = Y_M + x_a \tag{5.11}$$

- The orientation of the landmark is "Left" in the 2D grid map:

$$X_W = X_M + z_a \qquad Y_W = Y_M - x_a \tag{5.12}$$

with *(X_W, Y_W)* being the coordinates of the wheelchair in the OXY plane; *(X_M, Y_M)* is the coordinate of the landmark.

Assuming the virtual 2D grid map is depicted as in Figure 5.10e, the wheelchair's position (X_G, Y_G) in the virtual 2D grid map is:

$$X_G = n - round\left(\frac{Y_W}{a}\right) \qquad Y_G = round\left(\frac{X_W}{a}\right) - 1 \tag{5.13}$$

5.3. Navigating a electric wheelchair in the real environment

The wheelchair cannot move using simulated actions from DQNs due to its lack of a multi-directional control model. A new algorithm based on WAC is proposed for the wheelchair's movement, outlined in Figure 5.12.

(a) Converter with the simulated inputs and the actual outputs

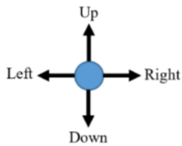

(b) Representation of four control directions

Figure 5.12. *The representation of converting actual control commands from the simulation.*

The action of the wheelchair, represented by a_w, and the new direction $d' = a$ during movement in the real environment need to be determined, as follows:

$$\begin{cases} a_w = \begin{cases} Forward & if \quad a = Up \\ Backward & if \quad a = Down \\ Left-Forward & if \quad a = Left \\ Right-Forward & if \quad a = Right \end{cases} \\ d = Up \end{cases} \tag{5.14a}$$

$$\begin{cases} a_w = \begin{cases} Forward & if \quad a = Left \\ Backward & if \quad a = Right \\ Left-Forward & if \quad a = Down \\ Right-Forward & if \quad a = Up \end{cases} \\ d = Left \end{cases} \tag{5.14c}$$

$$\begin{cases} a_w = \begin{cases} Forward & if \quad a = Down \\ Backward & if \quad a = Up \\ Left-Forward & if \quad a = Right \\ RightandForward & if \quad a = Left \end{cases} \\ d = Down \end{cases} \tag{5.14b}$$

$$\begin{cases} a_w = \begin{cases} Forward & if \quad a = Right \\ Backward & if \quad a = Left \\ Left-Forward & if \quad a = Up \\ Right-Forward & if \quad a = Down \end{cases} \\ d = Right \end{cases} \tag{5.14d}$$

In equations (5.14a) – (5.14d), the wheelchair actions a_w are defined as follows: a_w = *Forward* (move forward), a_w = *Backward* (move backward), a_w = *Left-Forward* (turn left and then move forward), a_w = *Right-Forward* (turn right and then move forward), a_w = *Stop* (come to a stop).

5.4. The obstacle avoidance method based on 3D environmental information

The 2D map is converted from the 3D point map using geometric projections. The transformation of the 2D map is calculated as follows:

$$Z_{imin} = min\left(Z_{ij}\right) \left(j = \overline{0, n}\right) \tag{5.15}$$

where the value Z_{imin} is chosen corresponding to the value *Yjmin* depending on the height of the wheelchair or the height of the wheelchair user.

To find the pixel with the minimum depth Z_{min} (closest to the camera), compare the Z_{imin} values in each column according to (5.16). The width a_v of the free space $(v = 1,2, \dots)$ in the 2D map (X_i, Z_{imin}) is calculated as (5.17).

$$Z_{min} = min(Z_{imin})\ (j = \overline{0, m}) \quad (5.16) \qquad a_v = |X_{k1} - X_{k2}| \quad (5.17)$$

with the values k_1 and k_2 being the first and last elements on the X-axis of the v^{th} gap at the column with depth $Z \geq Z_{min}$.

5.5. Experimental results of controlling the electric wheelchair

5.5.1. Simulation of training pathfinding for the wheelchair based on the virtual 2D grid map

Two virtual 2D grid maps of the indoor environment, depicted in Figure 5.15, are created. White cells represent empty spaces, black cells signify obstacles, and red cells denote goal points. Table 5.1 details the parameters used during training.

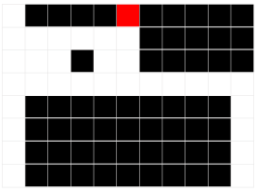

(a) 8 × 11 grid map

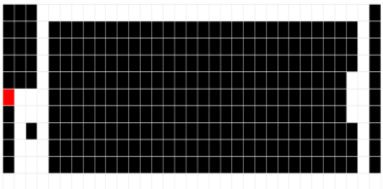

(b) 11 × 33 grid map

Figure 5.15. *Training environment.*

Table 5.1. *Training Parameters.*

Parameter	Value
Learning rate	0.00001
Discount factor γ	0.8
Exploration	0.1
Mini-batch size	32
Replay memory size	100
Reward when moving outside the map R_b	−0.8
Reward of free space R_f	−0.4
Reward of obstacle R_o	−0.75
Reward of goal R_g	1

Training results for the DQNs model are shown in Figures 5.16 and 5.17. A comparison of training time and the number of episodes for the DQNs model with two activation functions is presented in Table 5.2. Table 5.3 details the number of episodes and training time for two environments (Small and Large).

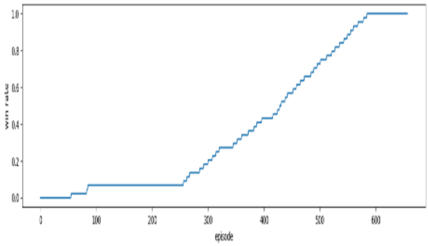

(a) The DQN model with PReLU activation

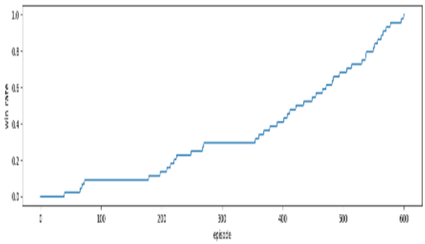

(b) The DQN model with ReLU activation

Figure 5.16. *The comparison of Win rates when training the DQN model with two activation types in the case of the 8 × 11 grid map.*

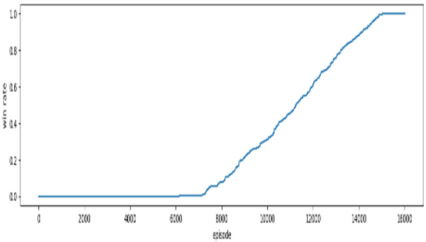

(a) The DQN model with PReLU activation

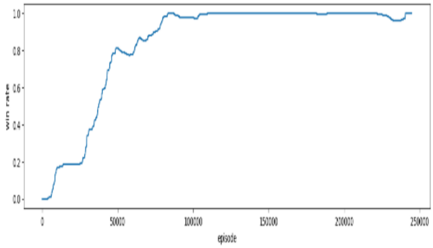

(b) The DQN model with ReLU activation

Figure 5.17. *The comparison of Win rates when training the DQN model with two activation types in the case of the 11 × 33 grid map.*

Table 5.2. *The Relative Performance of Proposed DQN Models.*

Environment	**Model**	**Average no. of Episodes**	**Average Training Time**
Small (8 × 11)	DQNs – ReLU	601	36,3 s
	DQNs – PreLU	657	42,3 s
Large (11 × 33)	DQNs – ReLU	244879	6,05 h
	DQNs – PreLU	16015	35,24 m

Bảng 5.3. *The Relative Performance of Previous Models.*

Environment	**Model**	**Average no. of Episodes**	**Average Training Time**
Small (8 × 11)	Traditional Q-Learning	60	198,4 s
	SARSA	75	223,9 s
Large (11 × 33)	Traditional Q-Learning	235	1,45 h
	SARSA	275	57,23 m

5.5.2. Results of landmark recognition

Figure 5.19 illustrates the identification of 4 landmarks using the SURF method. Table 5.4 shows the accuracy in landmark recognition, where *SF* is the number of feature points of the identified landmark, *TF* is the number of feature points matching the identified landmark, R_t is the accuracy rate, and R_f is the recognition error.

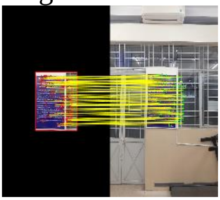

(a) Matching features of landmarks 1

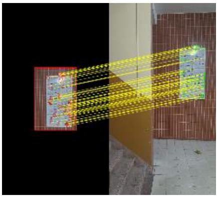

(b) Matching features of landmarks 2

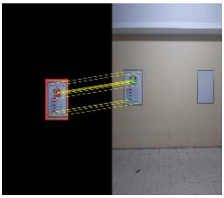

(c) Matching features of landmarks 3

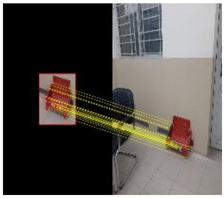

(d) Matching features of landmarks 4

(e) Landmark 1

(f) Landmark 2

(g) Landmark 3

(h) Landmark 4

Figure 5.19. *The representation of 4 different types of landmarks identified based on the landmarks stored in the database.*

Table 5.4. Accuracy of the identified landmarks using the SURF method.

Figure	Identification time (ms)	SF	TF	Rt (%)	Rf (%)
5.19a	370.6	206	190	92,2	7,8
5.19b	320.4	64	58	90,6	9,4
5.19c	296.9	18	13	72,2	27,8
5.19d	228.0	30	26	86,7	13,3

5.5.3. Determining the wheelchair's position on the virtual 2D grid map based on landmarks

Figure 5.20 illustrates distance measurement accuracy from the camera to the landmarks, while Figure 5.21 shows absolute error in distance measurement from the camera to the landmarks at varying distances along the vertical axis.

Figure 5.20. *Absolute error of the distance Xa measurement from the camera to the landmarks at different locations*

Figure 5.20. *Absolute error of the distance Za measurement from the camera to the landmarks at different locations*

The experiment took place in the environment depicted in Figure 5.22, with Figure 5.23 illustrating the wheelchair positions. Table 5.5 presents the results of wheelchair localization on the 2D grid map.

(a) Real environment (b) 2D grid map

Figure 5.22. *The indoor experimental environment.*

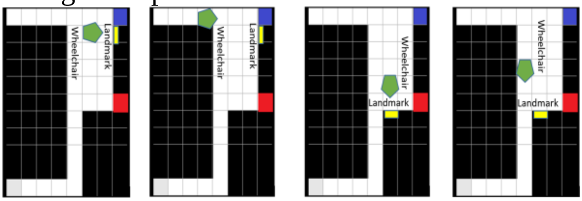

(a) The 1st position (b) The 2nd position (c) The 3rd position (d) The 4th position

Figure 5.23. *Four positions of the wheelchair on the 2D grid map with the landmarks.*

Table 5.5. Accuracy of positioning the wheelchair.

No.	Real position (X_0,Y_0)	Calculated position (X_W,Y_W)	$\lvert X_w-X_0\rvert$ (cm)	$\lvert Y_w-Y_0\rvert$ (cm)	Position on 2D grid map (X_{WG},Y_{WG})	Wheelchair direction on 2D grid map
1	(180, 720)	(182, 718)	2	2	(2,1)	Up
2	(60, 480)	(58, 477)	2	3	(4,0)	Up
3	(600, 660)	(596, 665)	4	5	(2,4)	Right
4	(480, 540)	(474, 538)	6	2	(3,3)	Right

Figure 5.24 depicts wheelchair and landmark positions, while Table 5.6 shows the results of wheelchair localization using 3 landmarks. [53].

Table 5.6. *Accuracy of positioning the wheelchair using 3 landmarks.*

No.	Real position (X0,Y0)	Calculated position (X_W,Y_W)	|Xw-X0| (cm)	|Yw-Y0| (cm)
1	(480, 540)	(489, 564)	8	14
2	(360, 540)	(348, 534)	12	6

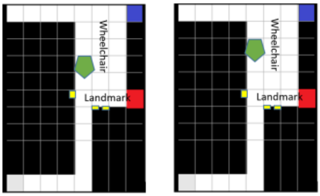

(a) Wheelchair at the position (3,3) (b) Wheelchair at the position (3,2)

Figure 5.24. *Positions of the wheelchair on the 2D grid map with 3 landmarks (yellow).*

5.5.4. The wheelchair moves to the desired destination based on the virtual 2D grid map

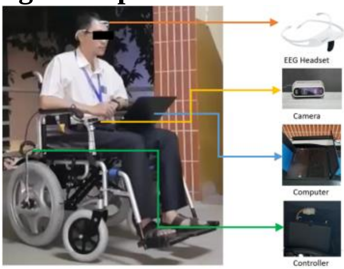

Figure 5.25. *The wheelchair navigation system installed with devices.*

The electric wheelchair, with an RGB-D camera system and other devices (Figure 5.25), undergoes experimentation in the depicted environment (Figure 5.26).

(a) Real environment

(b) Real environment

(c) Real environment

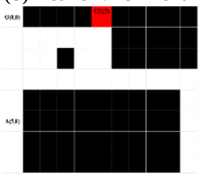

(d) The 2D grid map

Figure 5.26. *The experimental environment.*

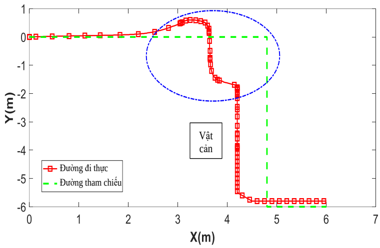

Figure 5.27. *The path of the wheelchair in the real environment.*

Figure 5.27 depicts the user-controlled path of the wheelchair using EEG signals [51]. The wheelchair's path in automatic mode is shown in Figure 5.29. The control commands are described in Table 5.7.

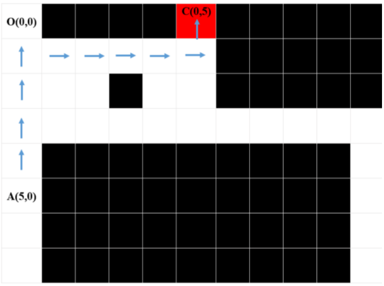

(a) The path of the green-arrow trajectory is simulated using DQNs

Table 5.7. *The wheelchair control commands are converted from simulated commands.*

State of Wheelchair	Current Direction D	Action of Model A	New Direction d'	Action of Wheelchair a_w
(5,0) to (4,0)	Up	Up	Up	Forward
(4,0) to (3,0)	Up	Up	Up	Forward
(3,0) to (2,0)	Up	Up	Up	Forward
(2,0) to (1,0)	Up	Up	Up	Forward
(1,0) to (1,1)	Up	Right	Right	Right–Forward
(1,1) to (1,2)	Right	Right	Right	Forward
(1,2) to (1,3)	Right	Right	Right	Forward
(1,3) to (1,4)	Right	Right	Right	Forward
(1,4) to (1,5)	Right	Right	Right	Forward
(1,5) to (0,5)	Right	Up	Up	Left–Forward

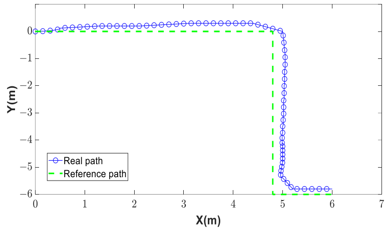

(b) Path of the wheelchair in the real environment using DQNs

Figure 5.29. *Representation of simulated and actual paths of the wheelchair using semi - automatic control.*

Figure 5.30a depicts three wheelchair trajectories. In Figure 5.30b, control commands are represented on the horizontal axis with values of -2, 0, 1, 2 corresponding to turn left, stop, go straight, and turn right commands. Another experiment is described in Figure 5.31. Figure 5.32 illustrates the differences between the wheelchair control methods in the second experimental environment.

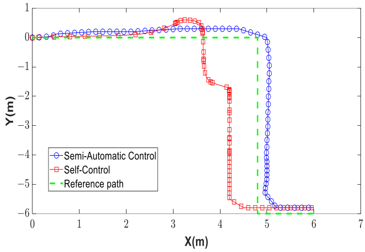

(a) The actual paths of both control methods and the reference path

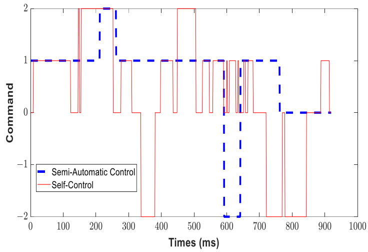

(b) The control commands of both methods

Figure 5.30. *Comparison of wheelchair movements between two control methods (semi - automatic control and manual control).*

(a) Real environment

(b) Real environment

(c) Real environment

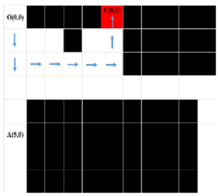

(d) The route simulated using DQNs.

Figure 5.31. *The environment in the second experiment.*

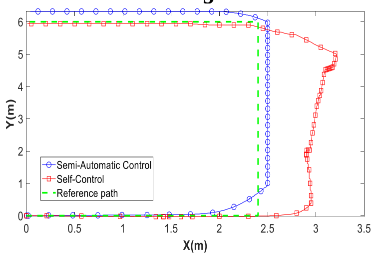

(a) The actual paths of both control methods and the reference path

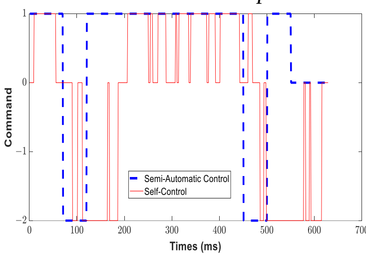

(b) The control commands of both methods

Figure 5.32. *Comparison of wheelchair movements between two control methods (semi - automatic control and manual control).*

Figure 5.33 depicts an experiment with obstacles appearing on the pre-planned path.

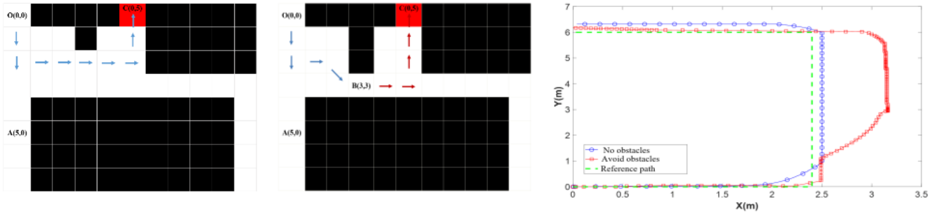

(a) Simulation path of the wheelchair without obstacle *(b) Simulation path of the wheelchair with an obstacle* *(c) The actual path of the wheelchair in the case of both with and without an obstacle*

Figure 5.33. *Motion of the wheelchair when there is an obstacle.*

CHAPTER 6: CONCLUSION AND FUTURE WORK

6.1. Conclusion

This dissertation successfully created an semi-automated electric wheelchair control system for indoor use by individuals with disabilities. It introduced two methods for classifying EEG signals based on eye movements in severely disabled individuals with functional eyes. The amplitude threshold method achieved high accuracy (97% and 99%) for different types of eye blinks. The CNN-1D model showed promising classification results (98.1%, 100%, 95.9%, 100%, 98.1%), offering scalability for diverse eye movement activities based on user communication needs with the computer or control system.

Moreover, the dissertation introduces the Maximum Feature Point Density method to identify natural landmarks and determine their positions based on the wheelchair's location and 3D information from a camera. It achieves the highest recognition accuracy (IOU > 0.8) within a distance of 2 meters from the camera. The landmark recognition process is fast, averaging 38.08 ms. Results indicate minimal errors in determining landmark positions—less than 3.0 cm horizontally and 2.0 cm vertically—when the camera-to-landmark distance is below 200 cm.

In conclusion, the dissertation proposes a virtual-real control model for indoor electric wheelchairs, integrating the DQNs-PreLU model for virtual 2D grid map navigation, a landmark-based localization method, and a real-world wheelchair navigation control. This model significantly reduces training time, approximately 5 times less than Q-Learning and SARSA, and nearly 12 times less than DQNs-ReLU. It also allows parameter set saving for real-world applications. Experimentally, the wheelchair exhibits minimal position errors and autonomously reaches the desired destination with a continuous trajectory, distinguishing itself from user-controlled navigation.

6.2. Future work

Given the swift progress of embedded systems on compact, high-speed computing platforms, the dissertation's algorithms and methods can further be explored and incorporated into specialized devices. This helps optimize connectivity and compatibility with existing wheelchairs while reducing costs.

REFERENCES

[1] "Global report on health equity for persons with disabilities," *World Health Organization,* pp. 1-312, 2022.

[2] "Điều tra Quốc gia về Người Khuyết tật tại Việt Nam," *Tổng cục Thống kê,* 2019.

[3] H. A. Lamti, P. Gorce, M. M. Ben Khelifa, and A. M. Alimi, "When mental fatigue maybe characterized by Event Related Potential (P300) during virtual wheelchair navigation," *Computer Methods in Biomechanics and Biomedical Engineering,* vol. 19, no. 16, pp. 1749-1759, 2016.

[4] "Electric Wheelchair Market - Growth, Trends, COVID-19 Impact, and Forecast (2022 - 2027)," *Mordor Intelligence,* pp. 1-90, 2022.

[5] N. T. Hai, "Development of a smart wheelchair using EEG technology and stereoscopic camera for disabled people," *International University,* vol. C2013-28-06, 2013.

[6] L. Q. Chuyên, "Mạng neural trong hệ thống điều khiển xe lăn cho người tàn tật nặng sử dụng điện não (EEG) và camera," *Luận Án Tiến Sĩ - Trường Đại Học Giao Thông Vận Tải Tp.HCM,* 2020.

[7] A. Lopes, J. Rodrigues, J. Perdigao, G. Pires, and U. Nunes, "A New Hybrid Motion Planner: Applied in a Brain-Actuated Robotic Wheelchair," *IEEE Robotics & Automation Magazine,* vol. 23, no. 4, pp. 82-93, 2016.

[8] Z. Li, S. Zhao, J. Duan, C. Y. Su, C. Yang, and X. Zhao, "Human Cooperative Wheelchair With Brain–Machine Interaction Based on Shared Control Strategy," *IEEE/ASME Transactions on Mechatronics,* vol. 22, no. 1, pp. 185-195, 2017.

[9] J. Tang, Y. Liu, D. Hu, and Z. Zhou, "Towards BCI-actuated smart wheelchair system," *BioMedical Engineering OnLine,* vol. 17, no. 1, pp. 1-22, 2018.

[10] H. N. Oon, A. Saidatul, and Z. Ibrahim, "Analysis on Non-Linear Features of Electroencephalogram (EEG) Signal for Neuromarketing Application," in *2018 International Conference on Computational Approach in Smart Systems Design and Applications (ICASSDA),* pp. 1-8, 2018.

[11] D.-K. Tran, T.-H. Nguyen, and T.-N. Nguyen, "Detection of EEG-Based Eye-Blinks Using A Thresholding Algorithm," *European Journal of Engineering and Technology Research,* vol. 6, no. 4, pp. 6-12, 2021.

[12] T. Nguyen, T. H. Nguyen, K. Q. D. Truong, and T. Van Vo, "A Mean Threshold Algorithm for Human Eye Blinking Detection Using EEG," in *4th International Conference on Biomedical Engineering in Vietnam*, Berlin, Heidelberg, pp. 275-279, 2013.

[13] H. T. Nguyen, N. Trung, V. Toi, and V. S. Tran, "An autoregressive neural network for recognition of eye commands in an EEG-controlled wheelchair," in *2013 International Conference on Advanced Technologies for Communications (ATC 2013),* pp. 333-338, 2013.

[14] A. Qayyum, M. K. A. A. Khan, M. Mazher, and M. Suresh, "Classification of EEG Learning and Resting States using 1D-Convolutional Neural Network for Cognitive Load Assesement," in *2018 IEEE Student Conference on Research and Development (SCOReD)*, pp. 1-5, 2018.

[15] U. R. Acharya, S. L. Oh, Y. Hagiwara, J. H. Tan, and H. Adeli, "Deep convolutional neural network for the automated detection and diagnosis of seizure using EEG signals," *Computers in Biology and Medicine,* vol. 100, pp. 270-278, 2018.

[16] A. N. Belkacem, N. Jamil, J. A. Palmer, S. Ouhbi, and C. Chen, "Brain Computer Interfaces for Improving the Quality of Life of Older Adults and Elderly Patients," *Frontiers in Neuroscience,* vol. 14, pp. 1-11, 2020.

[17] A. E. Hramov, V. A. Maksimenko, and A. N. Pisarchik, "Physical principles of brain–computer interfaces and their applications for rehabilitation, robotics and control of human brain states," *Physics Reports,* vol. 918, pp. 1-133, 2021.

[18] M. Dahmani *et al.*, "An Intelligent and Low-Cost Eye-Tracking System for Motorized Wheelchair Control," *Sensors,* vol. 20, no. 14, pp. 1-27, 2020.

[19] F. B. Taher, N. B. Amor, and M. Jallouli, "A multimodal wheelchair control system based on EEG signals and Eye tracking fusion," in *2015 International Symposium on Innovations in Intelligent SysTems and Applications (INISTA)*, pp. 1-8, 2015.

[20] C. Naijian, H. Xiangdong, W. Yantao, C. Xinglai, and C. Hui, "Coordination control strategy between human vision and wheelchair manipulator based on BCI," in *2016 IEEE 11th Conference on Industrial Electronics and Applications (ICIEA)*, pp. 1872-1875, 2016.

[21] R. J. M. G. Tello, A. L. C. Bissoli, F. Ferrara, S. Müller, A. Ferreira, and T. F. Bastos-Filho, "Development of a Human Machine Interface for Control of Robotic Wheelchair and Smart Environment," *IFAC-PapersOnLine*, vol. 48, no. 19, pp. 136-141, 2015.

[22] W. Jia, D. Huang, O. Bai, H. Pu, X. Luo, and X. Chen, "Reliable planning and execution of a human-robot cooperative system based on noninvasive brain-computer interface with uncertainty," in *2012 IEEE/RSJ International Conference on Intelligent Robots and Systems*, pp. 3798-3805, 2012.

[23] L. Xi and M. Shino, "Shared Control of an Electric Wheelchair Considering Physical Functions and Driving Motivation," *International Journal of Environmental Research and Public Health*, vol. 17, no. 15, 2020.

[24] J. Duan, Z. Li, C. Yang, and P. Xu, "Shared control of a brain-actuated intelligent wheelchair," in *Proceeding of the 11th World Congress on Intelligent Control and Automation*, pp. 341-346, 2014.

[25] A. M. Santana, K. R. T. Aires, R. M. S. Veras, and A. A. D. Medeiros, "An Approach for 2D Visual Occupancy Grid Map Using Monocular Vision," *Electronic Notes in Theoretical Computer Science,* vol. 281, pp. 175-191, 2011.

[26] W. Seo and K.-R. Baek, "Indoor Dead Reckoning Localization Using Ultrasonic Anemometer with IMU," *Journal of Sensors,* vol. 2017, pp. 1-12, 2017.

[27] H. Rashid and A. K. Turuk, "Dead reckoning localisation technique for mobile wireless sensor networks," *IET Wireless Sensor Systems,* vol. 5, no. 2, pp. 87-96, 2015.

[28] X. Zhang, S. Zhu, Z. Wang, and Y. Li, "Hybrid visual natural landmark–based localization for indoor mobile robots," *International Journal of Advanced Robotic Systems,* vol. 15, no. 6, pp. 1-18, 2018.

[29] G. Lee, B.-C. Moon, S. Lee, and D. Han, "Fusion of the SLAM with Wi-Fi-Based Positioning Methods for Mobile Robot-Based Learning Data Collection, Localization, and Tracking in Indoor Spaces," *Sensors,* vol. 20, no. 18, pp. 1-20, 2020.

[30] P. Viola and M. Jones, "Rapid object detection using a boosted cascade of simple features," in *Proceedings of the 2001 IEEE Computer Society Conference on Computer Vision and Pattern Recognition. CVPR 2001*, Kauai, HI, USA, pp. 511-518, 2001.

[31] D. G. Lowe, "Distinctive Image Features from Scale-Invariant Keypoints," *International Journal of Computer Vision,* vol. 60, no. 2, pp. 91-110, 2004.

[32] H. Bay, T. Tuytelaars, and L. Van Gool, "SURF: Speeded Up Robust Features," in *Computer Vision – ECCV 2006*, Berlin, Heidelberg, pp. 404-417, 2006.

[33] Y. Qian, H. Zheng, D. He, Z. Zhang, and Z. Zhang, "R-CNN Object Detection Inference With Deep Learning Accelerator," in *2018 IEEE/CIC International Conference on Communications in China (ICCC Workshops)*, pp. 297-302, 2018.

[34] C. Liu, Y. Tao, J. Liang, K. Li, and Y. Chen, "Object Detection Based on YOLO Network," in *2018 IEEE 4th Information Technology and Mechatronics Engineering Conference (ITOEC)*, pp. 799-803, 2018.

[35] E. H. C. Harik and A. Korsaeth, "The Heading Weight Function: A Novel LiDAR-Based Local Planner for Nonholonomic Mobile Robots," *Sensors,* vol. 19, no. 16, pp. 1-17, 2019.

[36] D. Foead, A. Ghifari, M. B. Kusuma, N. Hanafiah, and E. Gunawan, "A Systematic Literature Review of A* Pathfinding," *Procedia Computer Science,* vol. 179, pp. 507-514, 2021.

[37] A. I. Panov, K. S. Yakovlev, and R. Suvorov, "Grid Path Planning with Deep Reinforcement Learning: Preliminary Results," *Procedia Computer Science,* vol. 123, pp. 347-353, 2018.

[38] Y. Zhu *et al.*, "Target-driven visual navigation in indoor scenes using deep reinforcement learning," in *2017 IEEE International Conference on Robotics and Automation (ICRA)*, pp. 3357-3364, 2017.

[39] B.-V. Ngo, T.-H. Nguyen, D.-K. Tran, and D.-D. Vo, "Control of a Smart Electric Wheelchair Based on EEG Signal and Graphical User Interface for Disabled People," in *2021 International Conference on System Science and Engineering (ICSSE)*, pp. 257-262, 2021.

[40] B.-V. Ngo, T.-H. Nguyen, and T.-N. Nguyen, "EEG Signal-Based Eye Blink Classifier Using Convolutional Neural Network For BCI Systems," in *2021 15th International Conference on Advanced Computing and Applications (ACOMP)*, pp. 176-180, 2021.

[41] B.-S. N. Kleifges K, Kerick SE and Robbins KA, "BLINKER: Automated Extraction of Ocular Indices from EEG Enabling Large-Scale Analysis," *Frontiers in Neuroscience,* vol. 11, no. 12, pp. 1-17, 2017.

[42] M. Benda and I. Volosyak, "Peak Detection with Online Electroencephalography (EEG) Artifact Removal for Brain-Computer Interface (BCI) Purposes," *Brain Sci,* vol. 9, no. 12, pp. 1-21, 2019.

[43] B.-V. Ngo and T.-H. Nguyen, "Dense Feature-based Landmark Identification for Mobile Platform Localization," *International Journal of Computer Science and Network Security,* vol. 18, no. 12, pp. 186-200, 2018.

[44] E. Rublee, V. Rabaud, K. Konolige, and G. Bradski, "ORB: An efficient alternative to SIFT or SURF," in *2011 International Conference on Computer Vision*, pp. 2564-2571, 2011.

[45] X. Chai, F. Wen, and K. Yuan, "Fast vision-based object segmentation for natural landmark detection on Indoor Mobile Robot," in *2011 IEEE International Conference on Mechatronics and Automation*, pp. 2232-2237, 2011.

[46] P. Du and N. Bulusu, "An automated AR-based annotation tool for indoor navigation for visually impaired people," in *The 23rd International ACM SIGACCESS Conference on Computers and Accessibility*, Virtual Event, USA, pp. 1-4, 2021.

[47] J. G. Apud Baca *et al.*, "Automated Data Annotation for 6-DoF AI-Based Navigation Algorithm Development," *Journal of Imaging,* vol. 7, no. 11, pp. 236-253, 2021.

[48] O. Deane, E. Toth, and S.-H. Yeo, "Deep-SAGA: a deep-learning-based system for automatic gaze annotation from eye-tracking data," *Behavior Research Methods,* vol. 55, pp. 1372–1391, 2022.

[49] I. García-Aguilar, J. García-González, R. M. Luque-Baena, and E. López-Rubio, "Automated labeling of training data for improved object detection in traffic videos by fine-tuned deep convolutional neural networks," *Pattern Recognition Letters,* vol. 167, pp. 45-52, 2023.

[50] B.-V. Ngo and T.-H. Nguyen, "A Semi-Automatic Wheelchair with Navigation Based on Virtual-Real 2D Grid Maps and EEG Signals," *Applied Sciences*, vol. 12, pp. 1-20, 2022.

[51] B.-V. Ngo, T.-H. Nguyen, V.-T. Ngo, D.-K. Tran, and T.-D. Nguyen, "Wheelchair Navigation System using EEG Signal and 2D Map for Disabled and Elderly People," in *2020 5th International Conference on Green Technology and Sustainable Development (GTSD),* pp. 219-223, 2020.

[52] B.-V. Ngo and T.-H. Nguyen, "Positioning an electric wheelchair in 2D grid map based on natural landmarks for navigation using Q-Learning," *Indonesian Journal of Electrical Engineering and Computer Science,* vol. 31, no. 1, pp. 115-125, 2023.

[53] N. T. H. Nguyen Tan Nhu, "Landmark-Based Robot Localization Using a Stereo Camera System," *American Journal of Signal Processing,* vol. 5, no. 2, pp. 40-50, 2015.

LIST OF PUBLICATIONS

[1] **Ba-Viet Ngo,** Thanh-Hai Nguyen, Chi-Cuong Vu, " Automatic Labeling of Natural Landmarks for Wheelchair Motion Planning ", *Electronics*, vol. 12, pp. 1-20, 2023. (**SCIE - Q2 - IF 2.9**)

[2] **Ba-Viet Ngo,** Thanh-Hai Nguyen, "Positioning an electric wheelchair in 2D grid map based on natural landmarks for navigation using Q-Learning", *Indonesian Journal of Electrical Engineering and Computer Science*, vol. 31, pp. 115-125, 2023. (**Scopus-Q3**)

[3] **Ba-Viet Ngo,** Thanh-Hai Nguyen, "A Semi-Automatic Wheelchair with Navigation Based on Virtual-Real 2D Grid Maps and EEG Signals", *Applied Sciences*, vol.12, pp. 1-20, 2022. (**SCIE - Q2 - IF 2.7)**

[4] **Ba-Viet Ngo,** Thanh-Hai Nguyen, "Dense Feature-based Landmark Identification for Mobile Platform Localization", *International Journal of Computer Science and Network Security*, vol. 18, pp. 186-200, 2018 **(ESCI)**

[5] **Ba-Viet Ngo,** Thanh-Hai Nguyen, Thanh-Nghia Nguyen, "EEG Signal-Based Eye Blink Classifier Using Convolutional Neural Network For BCI Systems", *in Proceedings of 15th International Conference on Advanced Computing and Applications (ACOMP)*, pp. 176-180, 2022.

[6] Dang-Khoa Tran; Thanh-Hai Nguyen; **Ba-Viet Ngo**; Minh-Ly Lai; Thi-My-Kieu Ong; Thi-Minh Vu, Van-Minh Nguyen, "Evaluation Between Visual And Auditory EEG Responses On Upper Limb Movement in The Temporal and Spectral Domains," *in Proceedings of 6th International Conference on Green Technology and Sustainable Development (GTSD)*, pp. 817-824, 2022.

[7] **Ba-Viet Ngo**, Thanh-Hai Nguyen, Dang-Khoa Tran, Duc-Dung Vo, "Control of a Smart Electric Wheelchair Based on EEG Signal and Graphical User Interface for Disabled People", *in Proceedings of International Conference on System Science and Engineering (ICSSE)*, pp. 257-262, 2021.

[8] Dang-Khoa Tran, Thanh-Hai Nguyen, **Ba-Viet Ngo**, "Amplitude Thresholding of EEG Signals For Eye Blink and Saccade Detection", *in Proceedings of International Conference on System Science and Engineering (ICSSE)*, pp. 268-273, 2021.

[9] **Ba-Viet Ngo**, Thanh-Hai Nguyen, Van-Thuyen Ngo, Dang-Khoa Tran, Truong-Duy Nguyen, " Wheelchair Navigation System using EEG Signal and 2D Map for Disabled and Elderly People ", *in Proceedings of 5th International Conference on Green Technology and Sustainable Development (GTSD)*, pp. 219-223, 2020.

[10] **Ba-Viet Ngo,** Thanh-Hai Nguyen, Van-Thuyen Ngo, "Hands-free control of an electric wheelchair using face behaviors ", *in Proceedings of International Conference on System Science and Engineering (ICSSE)*, pp. 29-33, 2017.

[11] **Ba-Viet Ngo**, Thanh-Hai Nguyen, Duc-Dung Vo, "An MICP Algorithm for 3D Map Reconstruction Based on 3D Cloud Information of Landmarks", *European Journal of Engineering and Technology Research*, vol. 6, pp. 130-138, 2021.

[12] Thanh-Hai Nguyen**, Ba-Viet Ngo,** Thanh-Hai Quach, " Optimization of Transformation Matrix for 3D Cloud Mapping Using Sensor Fusion ", *American Journal of Signal Processing*, vol. 8, pp. 9-19, 2018.